sciendo

Polish Journal of Medical Physics and Engineering
The Journal of Polish Society of Medical Physics
ISSN 1898-0309, doi: 10.2478/pjmpe-2019-0028

December 2019
Vol 25, Issue 4

Scientific Paper

Investigation of fast neutron shielding properties of new polyurethane-based composites loaded with B_4C, BeO, WO_3, ZnO, and Gd_2O_3 micro- and nanoparticles

Asghar MESBAHI[1,2,a], Khatibeh VERDIPOOR[2], Farhad ZOLFAGHARPOUR[3] , Abdolali ALEMI[4]

[1]*Molecular Medicine Research Center, Institute of Biomedicine, Tabriz university of Medical Sciences, Tabriz, Iran*
[2]*Medical Radiation Sciences Research Team, Tabriz University of Medical Sciences, Tabriz, Iran*
[3]*Department of Physics, Faculty of Basic Sciences, University of Mohaghegh Ardabili, Ardabil, Iran*
[4]*Department of inorganic chemistry, Faculty of Chemistry, Tabriz University, Tabriz, Iran*
[a]*E-mail address: amesbahi2010@gmail.com*

(received 13 May 2019; revised 3 September and 9 October 2019; accepted 13 November 2019)

Abstract

The aim of the current research was to study the radiation shielding properties of polyurethane-based shielding materials filled with B_4C, BeO, WO_3, ZnO, and Gd_2O_3 particles against fast neutrons. The macroscopic cross sections of composites containing micro- and nanoparticles with a diameter of 10 µm and 50 nm were calculated using MCNPX (2.6.0) Monte Carlo code. The results showed that adding nano-scaled fillers to polyurethane matrix increases attenuation properties of neutron shields compared to micro-scaled fillers for intermediate and fast neutrons. Among the studied composites, WO_3 and Gd_2O_3 nano-composites presented higher neutron cross section compared to others.

Key words: nanoparticles; shielding; fast neutrons; Monte Carlo method.

Introduction

The application of ionizing radiation in industry and medicine has increased due to their potential benefits in different aspects of human life. However, the hazardous effects of ionizing radiation had been the main disadvantage for their medical and industrial utilizations. In accordance with the development of new techniques using ionizing radiation, the investigations on novel shielding materials such as concretes and flexible low weight materials have been conducted in recent years [1-5].

In recent years, the advent of nanoparticles as new materials in radiation shielding resulted in significant progress in fabrication of nano-based shields for photons and neutrons [1,2,6-8]. The majority of the investigations indicated that the nanoparticles improved attenuation coefficients of composites. Also, it was shown that photon and neutron energy, nanoparticle concentration and size of nanoparticles were effective parameters in the efficiency of nanoparticle-based shielding materials [9-11]. Several studies were investigated the effect of nano-materials on shielding properties of glasses [12,13]. Some of them also examined the attenuation effect of nanomaterials in concretes and bricks as shielding used in radiation therapy facilities [7,10]. And finally several reports in the literature can be found concerning the shielding effect of flexible nano- and microparticles-based sheets used in diagnostic radiology [6,8,14].

There is a wide range of materials that were investigated as nano- and microparticles fillers in the fabrication of new shielding materials for photon and neutron beams [11]. In the current study, several nano- and microparticles including B_4C, BeO, WO_3, ZnO, and Gd_2O_3 as potential candidates to make more efficient neutron attenuators were investigated by Monte Carlo method. The purpose was to provide comparative information on their neutron attenuating properties in the same simulation geometry and neutron energy.

Methods and Materials

Monte Carlo simulations

In the current study, we used MCNPX (2.6.0) MC code for simulation of neutron shields and calculation of macroscopic cross section of fast neutrons with designed shielding materials [15]. The simulation geometry consisted of a surface source of neutron with a radius of 3 mm, two cylinders made of lead with radius of 20 cm and length of 10 cm. A hole with radius of 5 mm and length of 5 cm was designed in each cylinder to provide location for the neutron source. The schematic representation of geometry is shown in **Figure 1**. These two cylinders made of lead were used as absorbers of scattered neutrons as well as collimators to provide the conditions for narrow beam geometry for attenuation measurements. The polyurethane-based composite with thickness of 5 cm width of

10 cm and length of 10 cm was located between neutron source and detector cell. The dimensions were derived from experimental setup but were configured for MC simulations. The importance of collimators for neutrons was set to 0.05 to reduce the running time for MC simulations. Also, to reduce MC run-time the importance of photon was considered zero and by this way no photon was generated by interaction of neutrons with other materials. No other variance reduction method was used in all the simulations. The distance between neutron source and detector cell was 50 cm. The detector cell was modeled as small cylindrical cell with radius of 5 mm and length of 5 cm. Thus, to score neutrons entering the detector cell, the F4 tally was used for scoring the flux of neutrons entering the detector cell. This tally calculates the particle flux in terms of particles per cm^2 per initial source particle. The statistical errors of MC results were less than 1% on average for all simulations. For MC simulations, the number of primary neutrons differed for different samples and approximately 10^7-10^8 neutrons were simulated using a personal desktop computer.

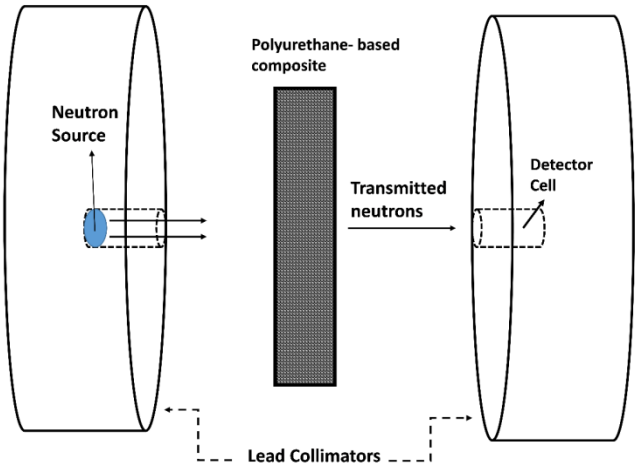

Figure 1. Schematic representation of the designed geometry in MCNPX code.

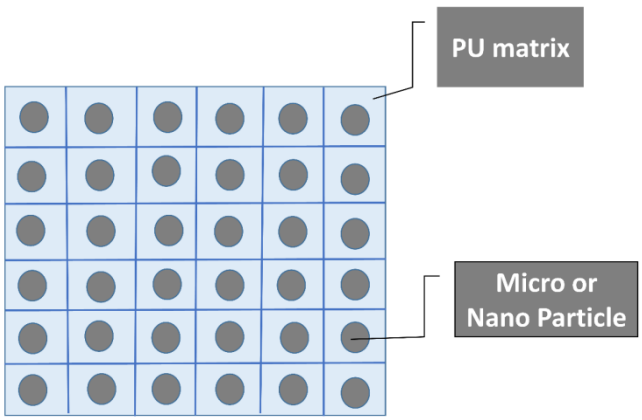

Figure 2. Geometry definition using lattice card in MCNPX code for micro- and nano-fillers in PU matrix.

The shielding material was a polyurethane matrix that was filled with different absorbing materials and various concentrations. The polyurethane matrix was selected for its easiness of fabrication and better mechanical and thermal properties. For MC simulation of composites, a polyurethane matrix with elemental composition of $C_{27}H_{36}N_2O_{10}$ and density of 0.96 g/cm^3 was used. The filler materials including Boron carbide, $^{10}B_4C$ (density = 2.52 g/cm^3), beryllium oxide, BeO (density of 3.02 g/cm^3), Tungsten trioxide, WO_3 (7.16 g/cm^3), zinc oxide, ZnO (5.61 g/cm^3) and Gadolinium *oxide* Gd_2O_3 (7.41 g/cm^3) were studied. Moreover, several concentrations of the above-mentioned materials including weight percentage (wt%) of 4.8, 9, 23, 37.5 were simulated. According to our experimental work the fabrication of samples with maximum concentration of 30 wt% of filler was feasible. However, the selection of studied concentrations was influenced by obtaining enough data and limitations existed in definition of different nano-sized materials in lattice card of MCNPX code. A mono-energetic parallel neutron beam with energies of 0.1, 0.3, 0.5, 1, 3, and 5 MeV was used for calculations. The criteria for energy selection were to analyze the shielding properties of our composites against the neutrons which were produced in medical linear accelerators in photon mode.

For a simulation of micro- and nanoparticles in MCNPX code, the Lattice and Universe cards were utilized. The shielding material was divided into small cells with variable dimensions in terms of µm and nm for micro and nanoparticle simulations. The size of these cells varied based on the studied concentrations of filler materials. Then each cell was filled with a sphere with diameter of 10 µm and 50 nm for micro and nanoparticle simulations respectively. The geometry was shown in **Figure 2**. For instance to provide 9% concentration of B_4C with a diameter of 50 nm in a polyurethane matrix, the dimension of cubic lattice cells was 0.002913 cm and a total number of nanoparticles in a shield with dimension of 3×4×4 cm reached 1.945×10^9. The neutron transmission for shielding materials with thickness of 3 cm was calculated using MC method. The selection of sample thickness was based on an approximate thickness of a shielding material that can cover the head of medical linear accelerator. The macroscopic cross sections of samples were obtained based on calculated transmission in two cases of with and without the sample using the following formula:

$$I = I_0\, e^{-\Sigma x} \qquad \text{Eq. 1}$$

where I_0 denotes the number of counted neutrons without the presence of absorber, I represents the number of counted neutrons that pass through a thickness (x) of a shielding material without undergoing any type of scattering or capture interaction. Also, Σ denotes the macroscopic cross section (cm^{-1}) which is defined as the probability of neutron interaction occurring per unit length of neutron travel through the shielding material. The mass macroscopic cross section of the sample can be calculated by dividing macroscopic cross section by the mass density of a composite and is expressed in terms of cm^2/g (see **Tables 1-6**).

Table 1. The comparison of neutron mass effective macroscopic cross section for micro- and nano-samples of B_4C at different energies (MeV).

Energy (MeV)	Samples		$\sum/\rho$ (cm^2/g) Micro	$\sum/\rho$ (cm^2/g) Nano	Diff %
0.1	4.8 wt% B_4C	95.2 wt% PU	0.598	0.672	3.04
	9 wt% B_4C	91 wt% PU	0.582	0.615	5.80
	23 wt% B_4C	77 wt% PU	0.5296	0.616	16.31
	37.5 wt% B_4C	62.5 wt% PU	0.486	0.615	26.68
0.3	4.8 wt% B_4C	95.2 wt% PU	0.417	0.434	4.19
	9 wt% B_4C	91 wt% PU	0.410	0.433	5.50
	23 wt% B_4C	77 wt% PU	0.387	0.433	11.92
	37.5 wt% B_4C	62.5 wt% PU	0.365	0.434	18.63
0.5	4.8 wt% B_4C	95.2 wt% PU	0.354	0.368	3.97
	9 wt% B_4C	91 wt% PU	0.350	0.368	5.07
	23 wt% B_4C	77 wt% PU	0.332	0.369	10.87
	37.5 wt% B_4C	62.5 wt% PU	0.317	0.368	16.27
1	4.8 wt% B_4C	95.2 wt% PU	0.166	0.172	3.47
	9 wt% B_4C	91 wt% PU	0.164	0.172	5.04
	23 wt% B_4C	77 wt% PU	0.156	0.172	10.64
	37.5 wt% B_4C	62.5 wt% PU	0.150	0.172	14.57
3	4.8 wt% B_4C	95.2 wt% PU	0.131	0.134	2.58
	9 wt% B_4C	91 wt% PU	0.131	0.137	4.72
	23 wt% B_4C	77 wt% PU	0.127	0.135	5.71
	37.5 wt% B_4C	62.5 wt% PU	0.126	0.135	6.93
5	4.8 wt% B_4C	95.2 wt% PU	0.102	0.105	2.73
	9 wt% B_4C	91 wt% PU	0.101	0.105	4.14
	23 wt% B_4C	77 wt% PU	0.098	0.105	6.58
	37.5 wt% B_4C	62.5 wt% PU	0.097	0.105	7.69

Table 2. The comparison of neutron mass effective macroscopic cross section for micro- and nano-samples of BeO at different energies (MeV).

Energy (MeV)	Samples		$\sum/\rho$ (cm^2/g) Micro	$\sum/\rho$ (cm^2/g) Nano	Diff %
0.1	4.8 wt% BeO	95.2 wt% PU	0.593	0.628	5.88
	9 wt% BeO	91 wt% PU	0.577	0.627	8.78
	23 wt% BeO	77 wt% PU	0.518	0.626	21
	37.5 wt% BeO	62.5 wt% PU	0.466	0.626	34.5
0.3	4.8 wt% BeO	95.2 wt% PU	0.411	0.434	5.64
	9 wt% BeO	91 wt% PU	0.402	0.432	7.61
	23 wt% BeO	77 wt% PU	0.370	0.433	17.11
	37.5 wt% BeO	62.5 wt% PU	0.336	0.433	28.63
0.5	4.8 wt% BeO	95.2 wt% PU	0.350	0.368	5.01
	9 wt% BeO	91 wt% PU	0.344	0.367	6.74
	23 wt% BeO	77 wt% PU	0.322	0.369	14.5
	37.5 wt% BeO	62.5 wt% PU	0.300	0.367	22.86
1	4.8 wt% BeO	95.2 wt% PU	0.327	0.339	3.69
	9 wt% BeO	91 wt% PU	0.324	0.338	4.25
	23 wt% BeO	77 wt% PU	0.308	0.339	10.05
	37.5 wt% BeO	62.5 wt% PU	0.287	0.340	18.39
3	4.8 wt% BeO	95.2 wt% PU	0.130	0.135	3.59
	9 wt% BeO	91 wt% PU	0.129	0.135	4.47
	23 wt% BeO	77 wt% PU	0.126	0.135	7.04
	37.5 wt% BeO	62.5 wt% PU	0.116	0.134	15.87
5	4.8 wt% BeO	95.2 wt% PU	0.101	0.106	4.33
	9 wt% BeO	91 wt% PU	0.100	0.105	5.3
	23 wt% BeO	77 wt% PU	0.095	0.105	9.92
	37.5 wt% BeO	62.5 wt% PU	0.092	0.105	13.63

Table 3. The comparison of neutron mass effective macroscopic cross section for micro- and nano-samples of Fe_3O_4 at different energies (MeV).

Energy (MeV)	Samples		$\sum/\rho$ (cm^2/g) Micro	$\sum/\rho$ (cm^2/g) Nano	Diff %
0.1	4.8 wt% Fe_3O_4	95.2 wt% PU	0.585	0.627	7.20
	9 wt% Fe_3O_4	91 wt% PU	0.560	0.697	11.95
	23 wt% Fe_3O_4	77 wt% PU	0.496	0.663	33.7
	37.5 wt% Fe_3O_4	62.5 wt% PU	0.425	0.626	47.43
0.3	4.8 wt% Fe_3O_4	95.2 wt% PU	0.408	0.435	6.74
	9 wt% Fe_3O_4	91 wt% PU	0.392	0.433	10.44
	23 wt% Fe_3O_4	77 wt% PU	0.347	0.434	25.12
	37.5 wt% Fe_3O_4	62.5 wt% PU	0.301	0.435	44.76
0.5	4.8 wt% Fe_3O_4	95.2 wt% PU	0.346	0.370	6.87
	9 wt% Fe_3O_4	91 wt% PU	0.332	0.3685	10.96
	23 wt% Fe_3O_4	77 wt% PU	0.293	0.370	26.09
	37.5 wt% Fe_3O_4	62.5 wt% PU	0.2517	0.3614	43.58
1	4.8 wt% Fe_3O_4	95.2 wt% PU	0.321	0.340	5.95
	9 wt% Fe_3O_4	91 wt% PU	0.311	0.344	10.59
	23 wt% Fe_3O_4	77 wt% PU	0.287	0.341	18.58
	37.5 wt% Fe_3O_4	62.5 wt% PU	0.262	0.339	29.26
3	4.8 wt% Fe_3O_4	95.2 wt% PU	0.127	0.135	6.28
	9 wt% Fe_3O_4	91 wt% PU	0.123	0.135	12.34
	23 wt% Fe_3O_4	77 wt% PU	0.112	0.135	20.58
	37.5 wt% Fe_3O_4	62.5 wt% PU	0.100	0.130	29.8
5	4.8 wt% Fe_3O_4	95.2 wt% PU	0.099	0.105	5.93
	9 wt% Fe_3O_4	91 wt% PU	0.097	0.105	8.17
	23 wt% Fe_3O_4	77 wt% PU	0.089	0.105	18.14
	37.5 wt% Fe_3O_4	62.5 wt% PU	0.082	0.105	28.65

Table 4. The comparison of neutron mass effective macroscopic cross section for micro- and nano-samples of WO_3 at different energies (MeV).

Energy (MeV)	Samples		$\sum/\rho$ (cm^2/g) Micro	$\sum/\rho$ (cm^2/g) Nano	Diff %
0.1	4.8 wt% WO_3	95.2 wt% PU	0.586	0.622	6.14
	9 wt% WO_3	91 wt% PU	0.566	0.626	10.75
	23 wt% WO_3	77 wt% PU	0.493	0.626	27.08
	37.5 wt% WO_3	62.5 wt% PU	0.418	0.625	49.51
0.3	4.8 wt% WO_3	95.2 wt% PU	0.403	0.434	7.7
	9 wt% WO_3	91 wt% PU	0.389	0.434	11.46
	23 wt% WO_3	77 wt% PU	0.304	0.434	27.7
	37.5 wt% WO_3	62.5 wt% PU	0.288	0.429	49.06
0.5	4.8 wt% WO_3	95.2 wt% PU	0.346	0.370	6.78
	9 wt% WO_3	91 wt% PU	0.334	0.369	10.47
	23 wt% WO_3	77 wt% PU	0.291	0.369	26.8
	37.5 wt% WO_3	62.5 wt% PU	0.246	0.365	48.15
1	4.8 wt% WO_3	95.2 wt% PU	0.320	0.336	5.15
	9 wt% WO_3	91 wt% PU	0.31	0.330	6.74
	23 wt% WO_3	77 wt% PU	0.281	0.340	21.03
	37.5 wt% WO_3	62.5 wt% PU	0.248	0.338	36.45
3	4.8 wt% WO_3	95.2 wt% PU	0.127	0.133	5.02
	9 wt% WO_3	91 wt% PU	0.12	0.135	9.57
	23 wt% WO_3	77 wt% PU	0.109	0.135	23.26
	37.5 wt% WO_3	62.5 wt% PU	0.096	0.134	40.02
5	4.8 wt% WO_3	95.2 wt% PU	0.099	0.104	5.24
	9 wt% WO_3	91 wt% PU	0.096	0.105	9.66
	23 wt% WO_3	77 wt% PU	0.085	0.105	22.46
	37.5 wt% WO_3	62.5 wt% PU	0.075	0.105	39.97

Table 5. The comparison of neutron mass effective macroscopic cross section for micro- and nano-samples of ZnO at different energies (MeV).

Energy (MeV)	Samples		$\sum/\rho$ (cm^2/g) Micro	$\sum/\rho$ (cm^2/g) Nano	Diff %
0.1	4.8 wt% ZnO	95.2 wt% PU	0.587	0.627	6.91
	9 wt% ZnO	91 wt% PU	0.566	0.627	10.75
	23 wt% ZnO	77 wt% PU	0.490	0.626	27.78
	37.5 wt% ZnO	62.5 wt% PU	0.435	0.626	44.09
0.3	4.8 wt% ZnO	95.2 wt% PU	0.406	0.435	7.03
	9 wt% ZnO	91 wt% PU	0.391	0.434	10.98
	23 wt% ZnO	77 wt% PU	0.339	0.434	27.97
	37.5 wt% ZnO	62.5 wt% PU	0.302	0.432	43.14
0.5	4.8 wt% ZnO	95.2 wt% PU	0.347	0.370	6.56
	9 wt% ZnO	91 wt% PU	0.334	0.369	10.37
	23 wt% ZnO	77 wt% PU	0.29	0.370	27.75
	37.5 wt% ZnO	62.5 wt% PU	0.257	0.367	42.81
1	4.8 wt% ZnO	95.2 wt% PU	0.320	0.340	6.18
	9 wt% ZnO	91 wt% PU	0.308	0.339	9.8
	23 wt% ZnO	77 wt% PU	0.267	0.355	32.56
	37.5 wt% ZnO	62.5 wt% PU	0.237	0.338	42.34
3	4.8 wt% ZnO	95.2 wt% PU	0.127	0.134	6.13
	9 wt% ZnO	91 wt% PU	0.123	0.135	9.9
	23 wt% ZnO	77 wt% PU	0.106	0.134	26.9
	37.5 wt% ZnO	62.5 wt% PU	0.095	0.135	42.31
5	4.8 wt% ZnO	95.2 wt% PU	0.099	0.105	5.84
	9 wt% ZnO	91 wt% PU	0.097	0.105	8.95
	23 wt% ZnO	77 wt% PU	0.083	0.105	25.5
	37.5 wt% ZnO	62.5 wt% PU	0.075	0.105	40.42

Table 6. The comparison of neutron mass effective macroscopic cross section for micro- and nano-samples of Gd_2O_3 at different energies (MeV).

Energy (MeV)	Samples		$\sum/\rho$ (cm^2/g) Micro	$\sum/\rho$ (cm^2/g) Nano	Diff %
0.1	4.8 wt% Gd_2O_3	95.2 wt% PU	0.589	0.6247	6.06
	9 wt% Gd_2O_3	91 wt% PU	0.565	0.6267	10.92
	23 wt% Gd_2O_3	77 wt% PU	0.498	0.6259	25.68
	37.5 wt% Gd_2O_3	62.5 wt% PU	0.424	0.6258	47.59
0.3	4.8 wt% Gd_2O_3	95.2 wt% PU	0.4086	0.4345	6.33
	9 wt% Gd_2O_3	91 wt% PU	0.3939	0.4348	10.35
	23 wt% Gd_2O_3	77 wt% PU	0.3458	0.4341	25.53
	37.5 wt% Gd_2O_3	62.5 wt% PU	0.2946	0.4352	47.72
0.5	4.8 wt% Gd_2O_3	95.2 wt% PU	0.3482	0.3697	6.17
	9 wt% Gd_2O_3	91 wt% PU	0.3346	0.3688	10.22
	23 wt% Gd_2O_3	77 wt% PU	0.2954	0.3699	25.22
	37.5 wt% Gd_2O_3	62.5 wt% PU	0.2514	0.3692	46.85
1	4.8 wt% Gd_2O_3	95.2 wt% PU	0.3214	0.3393	5.56
	9 wt% Gd_2O_3	91 wt% PU	0.3089	0.3392	9.8
	23 wt% Gd_2O_3	77 wt% PU	0.2772	0.3433	23.84
	37.5 wt% Gd_2O_3	62.5 wt% PU	0.2423	0.3383	39.62
3	4.8 wt% Gd_2O_3	95.2 wt% PU	0.1278	0.135	5.63
	9 wt% Gd_2O_3	91 wt% PU	0.1221	0.1347	10.31
	23 wt% Gd_2O_3	77 wt% PU	0.11	0.1351	22.81
	37.5 wt% Gd_2O_3	62.5 wt% PU	0.098	0.1347	37.44
5	4.8 wt% Gd_2O_3	95.2 wt% PU	0.0996	0.105	5.42
	9 wt% Gd_2O_3	91 wt% PU	0.0963	0.1056	9.65
	23 wt% Gd_2O_3	77 wt% PU	0.0861	0.1053	22.29
	37.5 wt% Gd_2O_3	62.5 wt% PU	0.0774	0.1051	35.78

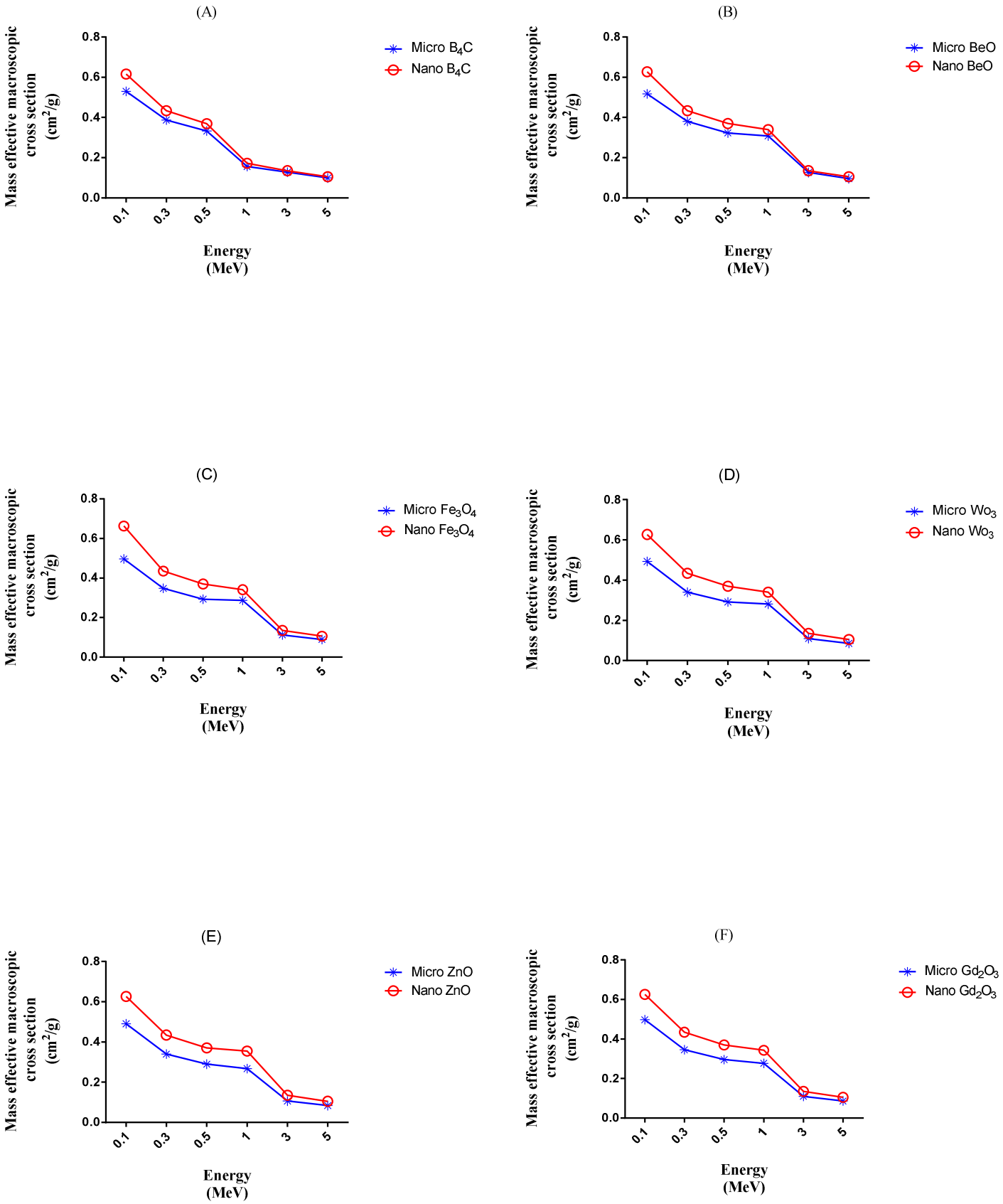

Figure 3. The comparison of mass effective macroscopic cross section (cm^2/g) of micro- and nano samples of neutron shielding containing 23.1wt% of fillers in terms of photon energy (MeV).

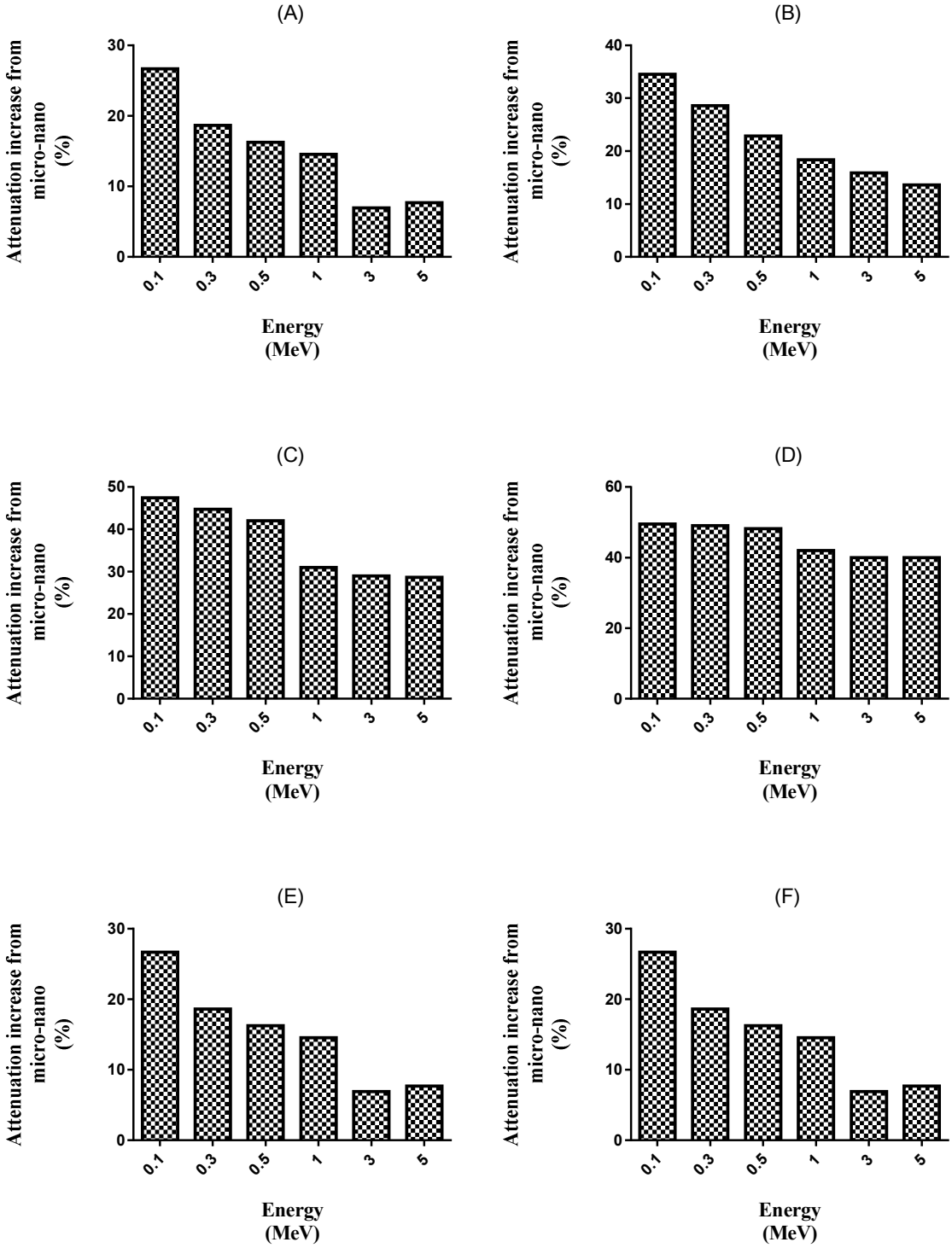

Figure 4. The assessment of attenuation increase from Micro to Nano state of samples containing 23.1 wt% of fillers in terms of neutron energy (MeV) (A). B_4C (B). BeO (C). Fe_3O_4 (D). WO_3 (E). ZnO (F). Gd_2O_3.

Results and Discussion

The comparison of neutron mass macroscopic cross section for micro and nano-based shields at different energies have been shown in **Tables 1-6**. For all composites, mass macroscopic cross sections were reduced with an increase in neutron energy. Nano-composites showed a higher attenuation effect relative to micro-composites depending on the filler concentration. In other words, for higher filler's concentration, the attenuation caused by a nano-filler was remarkably higher than its micro-filler counterpart.

For 0.1 MeV neutrons, the highest mass macroscopic cross section was seen for all studied composites. Moreover, for 0.1 MeV neutrons and concentration of 37.5 wt% of fillers, the values of mass macroscopic cross section were equal to 0.626 cm^2/g for all nano-composites, while for micro-composites it differed as 0.486 (B_4C), 0.466 (BeO), 0.425 (Fe_3O_4), 0.4185 (WO_3), 0.4185 (ZnO), 0.424 (Gd_2O_3) cm^2/g. The differences between nano and micro composites for all samples were between 25% and 49%. It was seen at the energy of 0.1 MeV and concentration of 37.5 wt% of fillers for all samples. It can be seen that the difference between nano and microparticles

was dependent on neutron energy, concentration of nanoparticles and filler type.

In **Figure 3**, the mass effective macroscopic cross section (cm^{-2}/g) was depicted for all studied samples. As can be seen, the shielding property of nanoparticle loaded samples was higher than microparticle- loaded samples. This superiority is increased with decreasing energy of neutrons from 5 MeV to 0.1 MeV. The maximum difference between nano- and micro-samples was about 49% for concentration of 0.375% and was found for WO_3 sample at the neutron energy of 0.1 MeV.

In **Figure 4**, the percentage of attenuation increase from nano-scaled sample to micro-scaled samples are shown for six studied shielding materials. As it was clearly shown that the magnitude of this increase was reduced by increasing the neutron energy from 0.1 to 5 MeV. However, the slope of this reduction was milder for WO_3 and Fe_3O_4 loaded samples compared to the other studied samples.

In **Figure 5** the percentage of increase in attenuation from micro to nanoscale has been depicted for samples with 37.5% wt of filler. Generally, this factor increases with increasing the density of fillers. For neutron energy of 0.3 MeV, WO_3 and Gd_2O_3 and ZnO nanoparticles have higher increase compared to others. For other energies 1 and 5 MeV, the superiority of WO_3 remains and small variations are seen between Gd_2O_3 and ZnO nanoparticles.

Considering the size effect of fillers, the results of the current study were similar to the finding of Adeli et al on thermal neutrons and shielding properties of B_4C/epoxy composite [9]. They showed that thermal neutron absorption was completely dependent on the size of the boron compound filler and addition of WO_3 increased the thermal neutron attenuation. However, it should be reminded here that in contrast to their experiments, we used fast neutrons and also the micro and nano-materials including WO3 and B4C/epoxy were evaluated separately as shielding sheets. Our results were consistent with the findings of Mesbahi et al who reported a higher attenuation for nano-filler compared to micro-sized fillers. They examined the shielding effect of doping ordinary concrete with PbO_2, Fe_2O_3, WO_3 and H_4B micro- and nanoparticle against fast neutrons [7]. The concrete doped with nanoparticles showed about 7% higher attenuation relative to microparticles.

The superiority of nanoparticles to microparticles is mainly attributed to the higher surface to volume ratio for nanoparticles compared to microparticles which increase the probability of interactions between neutrons and nanoparticles. Also, more homogenous composites can be made from nanoparticles compared to micro-fillers. This phenomenon is identical for both photons and neutrons and it has been reported in the previous studies [9-11,14,16-21]. However, it should be reminded here that most of the studies have been conducted on photon beams and a few reports have examined the neutron beam attenuation by nanoparticles. Thus, there were not many comparable results to be discussed here.

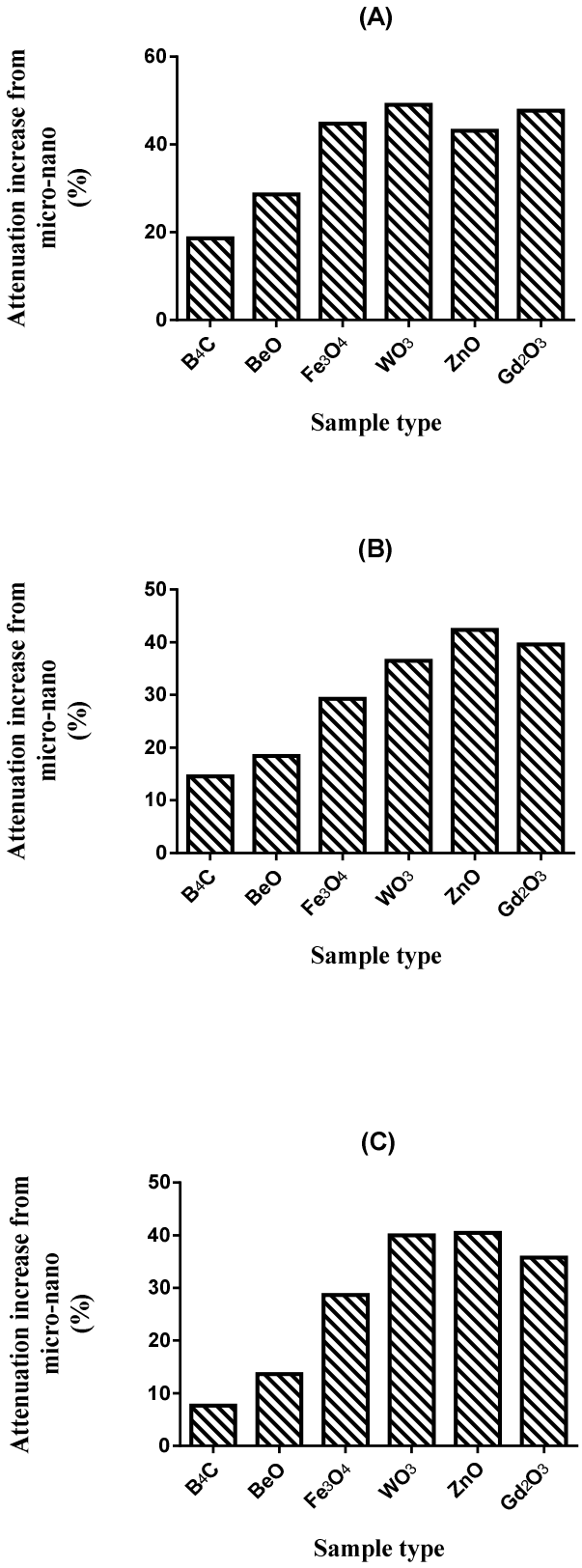

Figure 5. The assessment of attenuation increase from Micro to Nano state of samples containing 37.5 wt% of fillers at the energy of (A) 0.3 (B) 1.0 (C) 5.0 MeV.

Conclusion

In the current study, a comparative study was performed on several materials with a high attenuation effect on fast neutrons. It was found that nanoparticles of WO_3 and Gd_2O_3 and ZnO can be used as high neutron attenuating materials in fabrication of new shields for fast neutrons in a range of 0.1-5 MeV. Performing experimental studies based on the finding of the current study is recommended. Moreover, new investigations can be conducted on the fabrication of new composites made of a mixture of these nanomaterials.

Acknowledgements

The authors would like to thank Molecular Medicine Research Center of Tabriz University of Medical Sciences for their support.

References

[1] Aghaz A, Faghihi R, Mortazavi SMJ, et al. Radiation attenuation properties of shields containing micro and Nano WO3 in diagnostic X-ray energy range. Int J Radiat Res. 2016;14(2):127-131.

[2] Dong Y, Chang SQ, Zhang HX, et al. Effects of WO 3 particle size in WO_3/Epoxy resin radiation shielding material. Chinese Phys Letters. 2012;29(10):108102.

[3] Hu H, Wang Q, Qin J, et al. Study on composite material for shielding mixed neutron and gamma-rays. IEEE Trans Nucl Sci. 2008;55(4):2376-2384.

[4] Kim J, Seo D, Lee BC, et al. Nano-W dispersed gamma radiation shielding materials. Adv Eng Mater. 2014;16(9):1083-1089.

[5] Malekzadeh R, Mehnati P, Sooteh MY, Mesbahi A. Influence of the size of nano- and microparticles and photon energy on mass attenuation coefficients of bismuth-silicon shields in diagnostic radiology. Radiol Phys Technol. 2019;12(3):325-334.

[6] Li R, Gu Y, Wang Y, et al. Effect of particle size on gamma radiation shielding property of gadolinium oxide dispersed epoxy resin matrix composite. Mater Res Express. 2017;4(3):035035.

[7] Mesbahi A, Ghiasi H. Shielding properties of the ordinary concrete loaded with micro- and nano-particles against neutron and gamma radiations. Appl Radiat Isot. 2018;136:27-31.

[8] Mostafa AMA, Issa SAM, Sayyed MI. Gamma ray shielding properties of $PbO-B_2O_3-P_2O_5$ doped with WO_3. J Alloys Compounds. 2017;708:294-300.

[9] Adeli R, Shirmardi SP, Ahmadi SJ. Neutron irradiation tests on B_4C/epoxy composite for neutron shielding application and the parameters assay. Radiat Phys Chem. 2016;127:140-146.

[10] Tekin HO, Sayyed MI, Altunsoy EE, Manici T. Shielding properties and effects of WO3 and PbO on mass attenuation coefficients by using MCNPX code. Digest J Nanomaterials Biostructures. 2017;12(3):861-867.

[11] Verdipoor K, Alemi A, Mesbahi A. Photon mass attenuation coefficients of a silicon resin loaded with WO_3, PbO, and Bi_2O_3 Micro and Nano-particles for radiation shielding. Radiat Phys Chem. 2018;147:85-90.

[12] Dong MG, El-Mallawany R, Sayyed MI, Tekin HO. Shielding properties of $80TeO_2$-$5TiO_2$-(15-x) WO_3-xA_nO_m glasses using WinXCom and MCNP5 code. Radiat Phys Chem. 2017;141:172-178.

[13] El-Mallawany R, Sayyed MI. Comparative shielding properties of some tellurite glasses: Part 1.Physica B: Condensed Matter. 2017;539:133-140.

[14] Noor Azman NZ, Siddiqui SA, Hart R, Low IM. Effect of particle size, filler loadings and x-ray tube voltage on the transmitted x-ray transmission in tungsten oxide-epoxy composites. Appl Radiat Isot. 2013;71(1):62-67.

[15] Pelowitz DB. MCNPX user's manual version (2.6.0). LA-CP-07-1473. Los Alamos National Labratory, 2008.

[16] Lakshminarayana G, Baki SO, Kaky KM, et al. Investigation of structural, thermal properties and shielding parameters for multicomponent borate glasses for gamma and neutron radiation shielding applications. J Non-Crystalline Solids. 2017;471:222-237.

[17] Noor Azman NZ, Siddiqui SA, Low IM. Characterisation of micro-sized and nano-sized tungsten oxide-epoxy composites for radiation shielding of diagnostic X-rays. Mater Sci Eng C. 2013;33(8):4952-4957.

[18] Sayyed MI, Elmahroug Y, Elbashir BO, Issa SAM. Gamma-ray shielding properties of zinc oxide soda lime silica glasses. J Mater Sci: Mater Electron. 2017;28:4064-4074.

[19] Singh K, Singh S, Dhaliwal AS, Singh G. Gamma radiation shielding analysis of lead-flyash concretes. App Radiat Isot. 2015;95:174-179.

[20] Tekin HO, Singh VP, Manici T. Effects of micro-sized and nano-sized WO_3 on mass attenuation coefficients of concrete by using MCNPX code. Appl Radiat Isot. 2017;121:122-125.

[21] Tekin HO, Manici T. Simulations of mass attenuation coefficients for shielding materials using the MCNP-X code. Nucl Sci Tech. 2017;28:95-99.